

Lawrence Berkeley National Laboratory

LBL Publications

Title

Optical Waveguiding Charge-Transfer Cocrystals: Examining the Impact of Molecular Rotations on Their Photoluminescence.

Permalink

<https://escholarship.org/uc/item/86x4v98x>

Journal

Journal of the American Chemical Society, 147(10)

Authors

Navarro-Huerta, Armando

Matsuo, Takumi

Mikherdov, Alexander

et al.

Publication Date

2025-03-12

DOI

10.1021/jacs.4c15957

Peer reviewed

Optical Waveguiding Charge-Transfer Cocryystals: Examining the Impact of Molecular Rotations on Their Photoluminescence

Armando Navarro-Huerta, Takumi Matsuo, Alexander S. Mikherdov, Jan Blahut, Erika Bartůňková, Pingyu Jiang, Martin Dračinský, Simon Teat, Mingoo Jin,* Shotaro Hayashi,* and Braulio Rodríguez-Molina*



Cite This: *J. Am. Chem. Soc.* 2025, 147, 8343–8349



Read Online

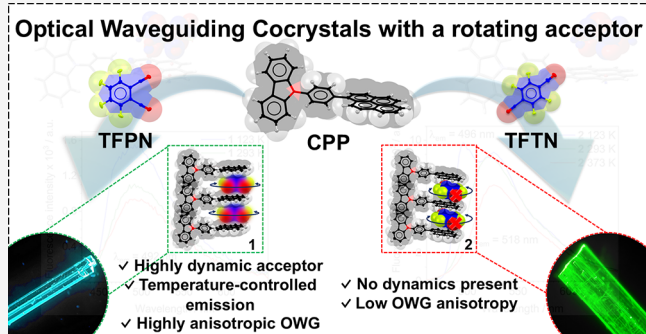
ACCESS |

Metrics & More

Article Recommendations

Supporting Information

ABSTRACT: Here, we present the first example of a binary optical waveguiding (OWG) cocrystal with large anisotropy featuring a fluorinated acceptor molecule (CPP-TFPN, **1**) with on-plane rotational dynamics, confirmed by solid-state NMR (^{19}F T_1) and theoretical calculations. Spatially resolved microphotoluminescence and variable-temperature photoluminescence experiments allowed us to examine the OWG performance and photophysical properties of both single crystals and bulk microcrystalline samples. A comparison with an analogous cocrystal containing a regioisomeric acceptor (CPP-TFTN, **2**) revealed that the photoluminescence characteristics of **1** are associated with the rotational motions of the acceptor, offering insights into how the molecular motion changes this property.



INTRODUCTION

The increasing demand for high-performance materials in optoelectronic devices has led to significant interest in organic cocryystals due to their ease of processing and lightweight nature. Unlike traditional crystalline materials, multicomponent systems provide customized morphological^{1–3} and photophysical^{4,5} properties by altering molecular combinations and stoichiometries.⁶ This approach takes advantage of the crystal engineering precepts through the complementary noncovalent interactions,⁷ ultimately leading to tunable emissive materials either by changing the initial materials⁸ or by fusing different crystalline materials following a lattice-mismatch heteroepitaxial strategy.^{9,10}

Notably, π -stacking is a crucial noncovalent interaction (NCI) implemented in multicomponent conjugated systems that plays a significant role in modulating the resulting photophysical properties.¹¹ The pairing of electron donors (D) and acceptors (A) often leads to solids exhibiting a red-shifted photoluminescence (PL) emission;¹² however, this combination can compromise the resulting PL intensity due to the facilitation of nonradiative pathways.^{13,14} Contrastingly, when a highly luminescent donor is combined with a mild electron-withdrawing fragment with a low tendency to form paramagnetic species, the PL is typically preserved.

The propagation of NCIs along specific crystallographic axes might result in anisotropic fluorescent single crystals capable of transmitting light in a specific direction, known as optical waveguides (OWGs),¹⁵ with potential application in nano-

photonics^{16,17} and data transmission.¹¹ Remarkable works of organic OWG materials based on cocryystals and molecular organic crystals have been reported using the directionality of the halogen^{18–20} and hydrogen^{21–23} bonds to propagate NCIs from the crystal packing both as one-²⁴ or two-dimensional²⁵ single crystals. However, the π -stacking provides a platform for the embedding of molecular fragments with different degrees of electron-accepting characteristics.²⁶

Our approach to fine-tuning and enhancing the photophysical properties of crystalline materials relies on the incorporation of molecular rotational motions within the structure via π -stacking of D/A pairs. It has been postulated that internal motions contribute to lattice relaxation via Brownian motion. For example, a recent study highlights that the molecular motion of small, symmetric fragments, like the 1,4-tetrafluorobenzoquinone component in a cocrystal, serves as a sink for radiative relaxation pathways, improving photothermal conversion properties.²⁷

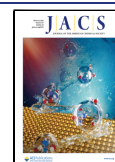
Tetrafluorophthalonitrile (TFPN) and tetrafluoroterephthalonitrile (TFTN) are small molecular building blocks previously used^{3,10} to assemble photoluminescent CT

Received: November 11, 2024

Revised: February 13, 2025

Accepted: February 14, 2025

Published: February 26, 2025



cocrystals due to their low degree of charge transfer character. Previously, it was reported that analogue tetrachlorophthalonitrile can display order–disorder phase transitions in CT cocrystals, which could be taken as the first approximation that other building blocks with smaller halogen atoms may show enhanced molecular motions, which could be evidenced by ^{19}F solid-state NMR.²⁸

RESULTS AND DISCUSSION

Structural Analysis and Crystal Morphology. In line with this reasoning, we present the characterization of two organic cocrystals: CPP-TFPN (1) and CPP-TFTN (2). As depicted in Figure 1, both were grown with the same

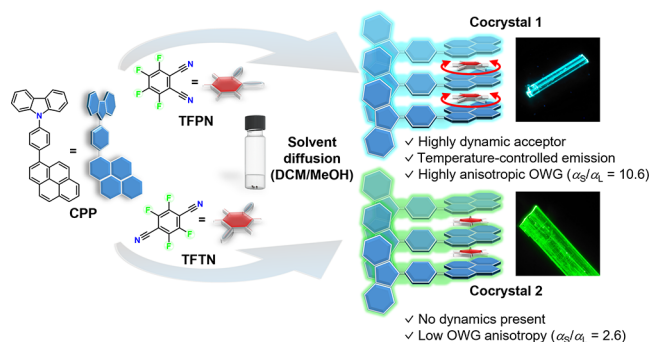


Figure 1. Synthesis of cocrystals with fluorinated acceptors to obtain organic optical waveguiding materials featuring tunable emission using a temperature stimulus via in-plane rotations of a small acceptor molecule.

fluorescent, polycyclic donor (CPP, after carbazole-phenylene-pyrene) through a liquid–liquid diffusion method (details of the synthesis of compound and crystallization are in the Supporting Information), yielding acicular single crystals. Under 254 nm UV light, cocrystal 1 produced turquoise-blue, fluorescent crystals, while cocrystal 2 displayed green fluorescence (Figure S5). Structural characterization was performed using variable-temperature single-crystal X-ray diffraction (VT SCXRD) using synchrotron radiation at 100,

200, and 300 K (Tables S1 and S2), revealing a 1:1 D/A stoichiometry in both cases. The interplanar distances between the pyrene core and the acceptors were 3.59 Å for 1 and 3.53 Å for 2 (Figure 2a,b).

The morphology of the crystals was further studied using the growth morphology method in Materials Studio. The calculated attachment energies (E_{att} ; Table S3, Figure S6) show that crystal growth occurs along the [100] crystallographic direction, consistent with the macroscopic shape of the single crystals. Additionally, energy framework calculations using CrystalExplorer 21.0,²⁹ featured in Figure S7, indicated similar D/A interaction energies in both solids, approximately -52 kJ/mol for 1 and -54 kJ/mol for 2.

Characterization of the Optical-Waveguiding Performance. Interestingly, under UV irradiation, the single crystals of both solids exhibited pronounced brightness at the tips, a characteristic feature of the OWG materials. To evaluate their performance, space-resolved microphotoluminescence (μPL) measurements were conducted at room temperature (details in the Supporting Information). To determine the facet for crystal irradiation, the transition dipole moments (TDMs) of the emissive CPP molecules were calculated in both systems; these vectorial quantities determine the probability of an electronic transition along a specific direction. The orientation of the resulting vectors, shown in Figure S8, is perpendicular to the π -stacking propagation between the donor and the fluorinated acceptors. Previous studies have shown that when the electric field vector of the incident light and the TDM of the chromophore are perpendicular, light reabsorption is maximized, improving waveguiding performance.³⁰

Photoirradiation experiments were conducted along both the long and short crystal axes with varying distances (D) between the excitation and waveguided positions, as depicted in the input images of Figure 2. Additional fluorescence images (Figure S9) display these distances. The recorded μPL spectra for both axes at the excitation and waveguiding positions, along with the crystal orientation, are shown in Figures S10 and S11.

The intensity ratios between waveguiding and excitation positions ($I_{\text{WG}}/I_{\text{EX}}$) were plotted (Figure 2c–f) and fitted using the relationship $I_{\text{WG}}/I_{\text{EX}} = A \exp(-\alpha D)$ to calculate the

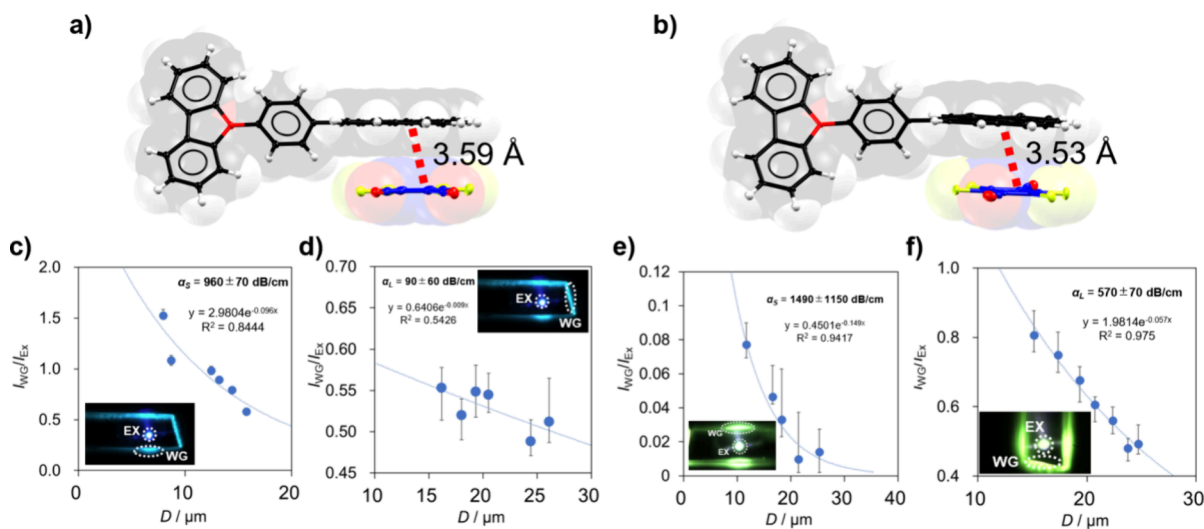


Figure 2. π -Stacking and D/A distances in (a) cocrystal 1 and (b) cocrystal 2. Ratios of emission intensity between excitation and waveguided positions in the long and short axes plotted as a function of the waveguided distance D for (c, d) cocrystal 1 and (e, f) cocrystal 2. Pictures of the measurements by the OWG in the crystals are indicated as insets in each plot ($\lambda_{\text{monitored}} = 500$ nm).

optical loss coefficients (α). For **1**, the loss coefficients are 960 ± 70 and 90 ± 60 dB cm⁻¹ for the short (α_S) and long axis (α_L), respectively. For **2**, the loss coefficients are $\alpha_S = 1490 \pm 1150$ dB cm⁻¹ and $\alpha_L = 570 \pm 70$ dB cm⁻¹. These values lie in the order of magnitude of previously reported OWG materials based on pyrene and carbazole.^{20,30–32}

The ratio of the loss coefficients (α_S/α_L) quantifies the degree of anisotropy in an OWG crystal.¹⁸ Based on the determined values, **1** exhibits an anisotropic waveguiding ability of 10.6, whereas for **2**, this parameter is 2.6. Recent reports^{22,30,33,34} on OWG crystalline materials imply that values $\alpha_S/\alpha_L > 3.9$ describe a highly anisotropic material with potential applications for highly regulated organic optical gates. The higher anisotropy in **1** (4-fold from **2**) may be attributed to slightly different directions of the TDM with respect to the incident electric field vector (Figure S8). Figure S12 displays overlapping of the absorption and emission spectra for both cocrystals. Cocrystal **1** portrays a 31% higher reabsorption than cocrystal **2**, which could be a feasible reason for the higher anisotropy of the OWG. Additional measurements of the α_L for cocrystal **2** (Figure S13) were performed using different laser wavelengths; nevertheless, the optical loss coefficient decreased, causing a change in the performance.

Variable-Temperature Photoluminescence Experiments in Polycrystalline Samples. Since μ PL measurements on single crystals cannot be performed at low temperatures due to technical limitations, we investigated further the emission of these cocrystals by variable-temperature PL experiments on bulk polycrystalline samples. First, the crystalline phase of the solids was confirmed through powder X-ray diffraction (PXRD) (Figure S14). The spectra of **1** (Figure 3a) confirmed the persistence of the emission maximum at 492 nm ($\lambda_{ex} = 372$ nm, CIE 0.064, 0.217, Figure S15) across the temperature range. The increasing PL intensity followed a trend inversely proportional to the temperature, as illustrated in Figure S16a, showing a linear 65% increase. In contrast, a new PL maximum emerged for **2** at 123 K (Figure 3c) with a wavelength of 496 nm ($\lambda_{ex} = 397$ nm, CIE 0.059, 0.829, Figure S15) compared to the 518 nm maximum observed at 293 and 373 K. The new maximum that is evident for **2** and barely noticeable for **1** may result from restricted molecular motions or freezing conformations at low temperatures, which enable new excited states, as suggested by Crespo-Otero et al.^{35–37} The PL intensity of **2** varied by 44% between the highest and lowest temperatures (Figure S16b), following a nonlinear trend, indicating a different PL relaxation process in this solid. Moreover, the PL quantum yields of the solids at room temperature were 23% ($\lambda_{ex} = 472$ nm) for cocrystal **1** and 26% ($\lambda_{ex} = 496$ nm) for cocrystal **2**.

Time-resolved decay measurements were performed to further investigate the PL of the solids. Figure 3b,d shows the decay curves for both cocrystals at 173, 293, and 373 K. The tail-fitting model revealed an average fluorescent lifetime (τ_{avg}) between 27 and 32 ns for **1**, while **2** showed significantly longer lifetimes between 62 and 69 ns. The complete fitting parameters are provided in Table S4. Single-crystal fluorescence micrographs were collected by using a LINKAM cryosystem to visualize these changes, confirming the PL intensity variations over the temperature range. These pictures are featured in Figure 3e.

Characterization of the Charge-Transfer Phenomena. Absorption spectroscopy using diffuse reflectance, highlighted in Figure S17a, revealed two broad absorptions, especially for

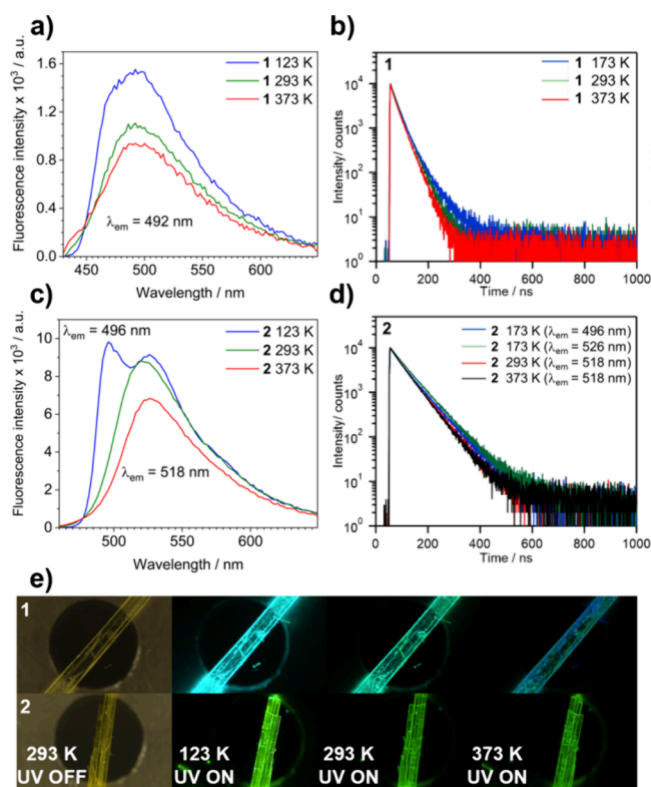


Figure 3. Variable-temperature comparative PL spectra of (a) cocrystal **1** and (c) **2** indicating the respective emission wavelength for the maxima. The time-resolved PL decay profiles of the cocrystals are depicted in panels b for **1** and d for **2** using a 375 nm pulse laser. (e) Single-crystal fluorescence micrographs at variable temperatures of cocrystals, highlighting the changes in PL emission.

cocrystal **2**. From these, the electronic optical gaps (E_g 's) were calculated using Tauc plots, yielding 2.93 eV for **1** and 2.47 eV for **2** (Figure S17b). These results suggest an intermolecular charge-transfer (ICT) effect between the D/A dyads, which is enhanced in cocrystal **2** due to the molecular symmetry of the acceptor,^{3,4} facilitating the electronic transitions from the donor to the acceptor. To confirm this, the ground-state geometries of the D/A dyads were optimized using density functional theory (DFT) and the Perdew–Burke–Erzenhof (PBE) functional.³⁸ The excited states and electronic transitions were then calculated using time-dependent (TD) DFT at the M06-2X³⁹/6-311G(d,p) level of theory in Gaussian09.⁴⁰ The results showed that the $S_0 \rightarrow S_1$ transition corresponds to an intermolecular charge-transfer state, with energies of 3.37 eV for **1** and 2.84 eV for **2**. A further calculation (Figure S31) with the dimer of cocrystal **1** and the TFPN rotated by 15° indicates that the change in the PL spectra can be attributed to slight changes in the conformations of the D/A components in the cocrystal. The natural transition orbitals (NTOs) involved are in the CPP and acceptor moieties, as depicted in Figure 4a. The NTOs of the starting materials were calculated at the same level of theory and are shown in Figure S18, pointing out a significant reduction in the energetic gap of the cocrystals compared to the starting materials.

Electron spin-resonance (ESR) spectroscopy in the solid state ruled out the presence of long-lived paramagnetic species even at temperatures as low as 77 K, as shown in Figure S19. It has been reported that the relaxation times of radical species

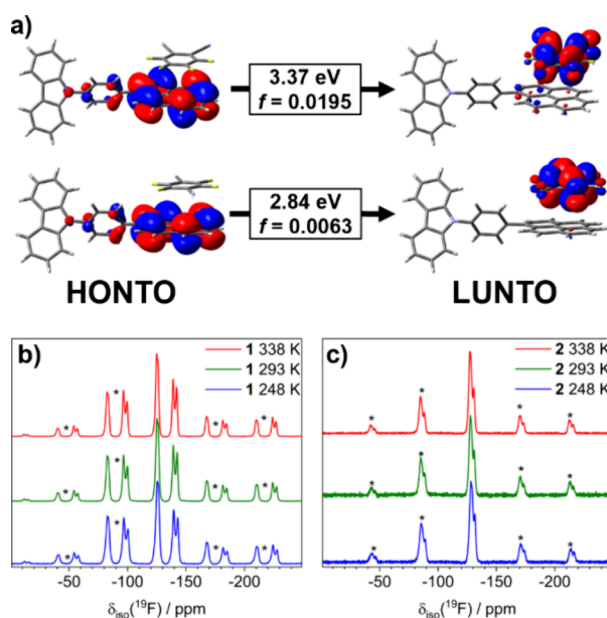


Figure 4. (a) Frontier natural transition orbitals for dyads of the cocrystals (up: 1; down: 2) at the M06-2X/6-311(d,p) level of theory with the energy associated with the $S_0 \rightarrow S_1$ transition and oscillator strength (f). VT ssNMR ^{19}F MAS spectra of cocrystals (b) 1 and (c) 2. The acquisition parameters are indicated in the Supporting Information. The asterisk indicates the spinning sidebands of the central set of signals (20 kHz).

can be highly affected due to the presence of molecular motions,⁴¹ as shall be described further in this work. Moreover, the degree of CT (ρ), a measurement of the ionicity of crystalline materials, was calculated through measurements of bond distances in SC XRD structures,⁵ revealing values of 0.035e and 0.100e for cocrystals 1 and 2, respectively. The results are condensed in Table S5 and are consistent with our experimental evidence through UV–vis spectroscopy. Additionally, the Fourier-transformed infrared (FTIR) spectra of the cocrystals further confirmed the low degree of ICT, inferred from the minimal shifts in the $\text{C}\equiv\text{N}$ stretching bands of the cyano groups compared to the starting materials, consistent with previous reports (Figures S20 and S21).^{42,43}

The changes in PL intensity across the temperature range prompted us to explore the feasibility of nonradiative pathways, specifically through molecular motions of small, symmetric fragments. A precedent by Garcia-Garibay et al. demonstrated that thermally driven molecular motions of a rotating fragment can detrimentally affect PL intensity in crystalline solids.⁴⁴

Assessment of the Molecular Motion through Solid-State NMR. To assess molecular motions in cocrystals 1 and 2, we examined the variable-temperature single-crystal X-ray diffraction and NMR data for both solids. First, the thermal stability of the cocrystals was studied through differential scanning calorimetry coupled with thermogravimetric analysis (DSC/TGA), depicted in Figure S22. Then, solid-state nuclear magnetic resonance (ssNMR) spectroscopy was carried out. The resulting ^{19}F MAS (magic-angle spinning) spectra (Figure 4b,c) at variable temperatures revealed no significant differences in the pattern and chemical shifts of the fluorinated acceptors. The three main sets of signals for 1 appeared at -125.6 , -139.5 , and -143.0 ppm, while for 2, they were at -128.3 and -131.5 ppm. Additionally, the cross-polarization

(CP MAS) pulse sequence on ^{13}C nuclei shows a series of aromatic signals ($\delta(^{13}\text{C}) > 100$ ppm) in both solids, as featured in Figure S23.

Regarding the SC XRD data, we observed that increasing the temperature leads to a more pronounced elongation and size variation in the thermal ellipsoids of the acceptor molecules in 1 compared to its TFTN analog. The deformation of the ellipsoids around the fluorine atoms occurs tangentially to the acceptor molecule, as shown in Figure 5a.

^{19}F T_1 Relaxation Measurements and Calculated Energy Barriers. As previously reported by Beckmann et

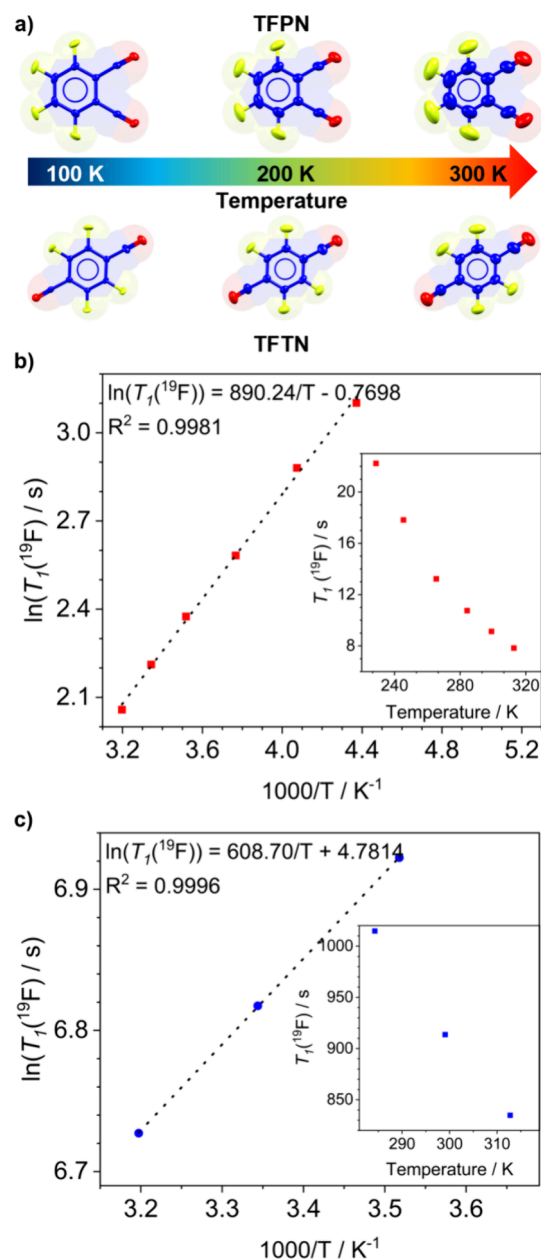


Figure 5. (a) Comparison of the elongation of the thermal ellipsoids in the TFPN and TFTN acceptor fragments in cocrystals 1 and 2, respectively, along the temperature interval. Thermal ellipsoids were drawn at the 50% level probability. Arrhenius plots using ^{19}F T_1 relaxation times through ssNMR saturation-recovery experiments in (b) cocrystal 1 and (c) cocrystal 2. As insets are depicted, the T_1 times vary as a function of the temperature for each graph.

al.^{45,46} and us,²⁷ molecular localized motions of fluorinated fragments can be studied through saturation-recovery experiments, which determine the ¹⁹F T_1 values. Using the Arrhenius equation to plot relaxation times as a function of temperature, $\ln(T_1) = E_a/RT + \ln(A)$, we constructed the graphs in Figure S5b,c. Due to the high relaxation times of the TFTN cocrystal, only three T_1 measurements were collected. In contrast, the relaxation behavior of **1** did not display the minimum associated with the concordance between rotational motion frequencies and the Larmor frequency of the spectrometer. Further measures would require a broader temperature range, which is currently beyond the capacity of the employed spectrometer. Also, the behaviors of the T_1 times as a function of the temperature are summarized in Table S6 and depicted as insets, showing distinct behaviors in the two cocrystals, with the relaxation times for **1** being up to 2 orders of magnitude shorter than those in **2**. The differences in the T_1 relaxation rates between cocrystals indicate distinct molecular dynamics due to different molecular microenvironments surrounding the fluorine atoms.

The rotational energy profiles of the two acceptors were also determined by using optimized geometries of molecular clusters through DFT calculations with the B3LYP functional. The resulting profiles are shown in Figures S24 and S25. For the TFPN in cocrystal **1**, the geometry optimizations provided two local minima corresponding to +60 and -60° rotation from the global minimum at 0° and relatively low rotational barriers of 5.9 and 7.4 kcal/mol. In contrast, for cocrystal **2**, only one minimum at -60° was found with a rotational barrier of 17.5 kcal/mol. These calculations support the experimental data indicating that the rotation of TFPN in cocrystal **1** is allowed and that the noncovalent interactions and steric hindrance in **2** (Figures S26 and S27) significantly hinder the in-plane rotation of TFTN.

Finally, to assess the possible contributions of the phenylene rings in the CPP core to overall dynamics, we performed ssNMR experiments on phenylene-deuterated cocrystals **1-d₄** and **2-d₄** using quadrupolar spin-echo measurements for ²H nuclei. The resulting spectra for both cocrystals, shown in Figures S28 and S29, display a typical Pake pattern, indicating the absence of molecular rotations within the time scale for this nucleus (10⁴–10⁷ Hz).⁴⁷ Additionally, an analysis of the NCI around the phenylene revealed significant steric hindrance with the surrounding CPP molecules, as shown in Figure S30.

CONCLUSIONS

This work provides a comprehensive analysis of two new CT cocrystals with great OWG properties. Cocrystal **1** exhibits anisotropy up to 4 times higher than that of cocrystal **2** due to the orientation of the transition dipole moment and higher reabsorption favored by its crystal packing. Notably, a significant and linear increase in photoluminescence (PL) at 123 K in cocrystal **1** can be attributed to the reduction of the in-plane rotational motion of its TFPN component at low temperatures, as supported by extensive solid-state NMR relaxation measurements and DFT calculations. These findings set a precedent for cocrystals with excellent OWG and thermally driven photoluminescent properties, suitable for applications such as optically regulated gates.

ASSOCIATED CONTENT

Supporting Information

The Supporting Information is available free of charge at <https://pubs.acs.org/doi/10.1021/jacs.4c15957>.

Synthetic and experimental procedures; ¹H and ¹³C NMR spectra of compounds; microscope photographs; thermal analyses; theoretical calculations; ssNMR ¹³C CP MAS, VT ¹⁹F MAS, and VT ²H NMR spectra; ¹⁹F T_1 relaxation times; final crystallographic refinement parameters; PXRD diffractograms; Tauc plots; PL model fittings; VT solid-state ESR; and room temperature FTIR spectra (PDF)

Accession Codes

Deposition numbers 2353024–2353029 contain the supplementary crystallographic data for this paper. These data can be obtained free of charge via the joint Cambridge Crystallographic Data Centre (CCDC) and Fachinformationszentrum Karlsruhe [Access Structures service](#).

AUTHOR INFORMATION

Corresponding Authors

Mingoo Jin – Institute for Chemical Reaction Design and Discovery (WPI-ICReDD), Hokkaido University, Sapporo, Hokkaido 060-8628, Japan; orcid.org/0000-0001-6199-8802; Email: mingoo@icredd.hokudai.ac.jp

Shotaro Hayashi – School of Engineering Science, Kochi University of Technology, Kami, Kochi 782-8502, Japan; FOREST Center, Research Institute, Kochi University of Technology, Kami, Kochi 782-8502, Japan; orcid.org/0000-0001-8703-6740; Email: hayashi.shotaro@kochi-tech.ac.jp

Braulio Rodríguez-Molina – Instituto de Química, Universidad Nacional Autónoma de México, Mexico City 04510, Mexico; orcid.org/0000-0002-1851-9957; Email: brodriguez@iquimica.unam.mx

Authors

Armando Navarro-Huerta – Instituto de Química, Universidad Nacional Autónoma de México, Mexico City 04510, Mexico; orcid.org/0000-0002-4144-894X

Takumi Matsuo – School of Engineering Science, Kochi University of Technology, Kami, Kochi 782-8502, Japan; orcid.org/0000-0002-0874-4798

Alexander S. Mikherdov – Institute for Chemical Reaction Design and Discovery (WPI-ICReDD), Hokkaido University, Sapporo, Hokkaido 060-8628, Japan; orcid.org/0000-0002-6471-5158

Jan Blahut – Institute of Organic Chemistry and Biochemistry, Czech Academy of Sciences, Prague 160 00, Czech Republic; orcid.org/0000-0001-7752-8370

Erika Bartůňková – Institute of Organic Chemistry and Biochemistry, Czech Academy of Sciences, Prague 160 00, Czech Republic

Pingyu Jiang – Institute for Chemical Reaction Design and Discovery (WPI-ICReDD), Hokkaido University, Sapporo, Hokkaido 060-8628, Japan

Martin Dračinský – Institute of Organic Chemistry and Biochemistry, Czech Academy of Sciences, Prague 160 00, Czech Republic

Simon Teat – Advanced Light Source, Lawrence Berkeley National Laboratory, Berkeley, California 94720-8229, United States

Complete contact information is available at:
<https://pubs.acs.org/10.1021/jacs.4c15957>

Notes

The authors declare no competing financial interest.

ACKNOWLEDGMENTS

This work was supported by the following projects: DGAPA PAPIIT IN207222, CONAHCYT Ciencia de Frontera 1715644, and the Ministry of Education, Youth, and Sports of the Czech Republic through the e-INFRA CZ (ID:90254). A.N.-H. acknowledges the support of CONAHCYT through a PhD scholarship (957838). We acknowledge the technical assistance from Dr. Ma. C. García González and Dr. F. J. Pérez Flores (MS); Dr. M. E. García Aguilera (ssNMR); M. A. Peña González, BSc, E. Huerta Salazar, MSc, Dr. I. Chavez, Dr. R. Gaviño, and Dr. B. Quiroz (solution NMR); A. Núñez Pineda, MSc (DSC/TGA), Dr. U. Hernández Balderas, and Dr. M. Tapia Tapia (PXRD); Dr. A. Romo Pérez (FTIR); Dr. R. A. Toscano (SC XRD); M. P. Orta Pérez (combustion analysis); and V. Gómez Vidales, MSc (ESR). We thank Dr. Y. A. Amador Sánchez and Dr. Diego Solis for access to ssUV-vis instruments. This research used resources of the Advanced Light Source, which is a DOE Office of Science User Facility under contract DE-AC02-05CH11231. We are also thankful for access to MIZTLI under project LANCAD-UNAM-DGTIC-392.

REFERENCES

- (1) Wu, B.; Zhuo, M.; Chen, S.; Su, Y.; Yu, Y.; Fan, J.; Wang, Z.; Wang, X. Controlling Morphological Dimensions of Organic Charge-Transfer Cocrystal by Manipulating the Growth Kinetics for Optical Waveguide Applications. *Adv. Opt. Mater.* **2023**, *11* (12), No. 2202895.
- (2) Ye, X.; Liu, Y.; Guo, Q.; Han, Q.; Ge, C.; Cui, S.; Zhang, L.; Tao, X. 1D versus 2D Cocrystals Growth via Microspacing In-Air Sublimation. *Nat. Commun.* **2019**, *10* (1), 761.
- (3) Sun, Y.; Lei, Y.; Hu, W.; Wong, W.-Y. Epitaxial Growth of Nanorod Meshes from Luminescent Organic Cocrystals via Crystal Transformation. *J. Am. Chem. Soc.* **2020**, *142* (16), 7265–7269.
- (4) Ma, Y.-X.; Wei, G.-Q.; Chen, S.; Lin, H.-T.; Wang, X.-D. Self-Assembled Organic Homostructures with Tunable Optical Waveguides Fabricated via “Cocrystal Engineering. *Chem. Commun.* **2021**, *57* (89), 11803–11806.
- (5) Barman, D.; Annadhasan, M.; Bidkar, A. P.; Rajamalli, P.; Barman, D.; Ghosh, S. S.; Chandrasekar, R.; Iyer, P. K. Highly Efficient Color-Tunable Organic Co-Crystals Unveiling Polymorphism, Isomerism, Delayed Fluorescence for Optical Waveguides and Cell-Imaging. *Nat. Commun.* **2023**, *14* (1), 6648.
- (6) Zhang, J.; Zhao, S.; Jiang, J.; Lv, Z.; Luo, J.; Shi, Y.; Lu, Z.; Wang, X. Organic Cocrystal Alloys: From Three Primary Colors to Continuously Tunable Emission and Applications on Optical Waveguides and Displays. *Small* **2024**, *20* (33), No. 2400313.
- (7) Sun, L.; Wang, Y.; Yang, F.; Zhang, X.; Hu, W. Cocrystal Engineering: A Collaborative Strategy toward Functional Materials. *Adv. Mater.* **2019**, *31* (39), No. 1902328.
- (8) Lv, Q.; Wang, X. D.; Yang, W. Y.; Wang, K. L.; Xu, C. F.; Zheng, M.; Liao, L. S. A General Synthetic Approach of Organic Lateral Heterostructures for Optical Signal Converters in All-Color Wavelength. *CCS Chemistry* **2023**, *5* (2), 423–433.
- (9) Lv, Q.; Wang, X. D.; Yu, Y.; Zhuo, M. P.; Zheng, M.; Liao, L. S. Lattice-Mismatch-Free Growth of Organic Heterostructure Nanowires from Cocrystals to Alloys. *Nat. Commun.* **2022**, *13* (1), 1–10.
- (10) Lv, Q.; Wang, X. D.; Yu, Y.; Yu, Y. J.; Zheng, M.; Liao, L. S. Selective Epitaxial Growth of Organic Heterostructure via Cocrystal Engineering: Towards Oriented Signal Conversion. *Sci. China Mater.* **2023**, *66* (10), 3968–3976.
- (11) Qi, Z.; Ma, Y.; Yan, D. One-dimensional Molecular Co-crystal Alloys Capable of Full-color Emission for Low-loss Optical Waveguide and Optical Logic Gate. *Aggregate* **2023**, *5* (1), No. e411.
- (12) Chen, Q.; Chen, X.; Han, Y.; Zhang, T.; Li, C.-P.; Mu, J.; Zhang, J.; Hao, J.; Xue, P. Multistimuli-Responsive Fluorescent Switches Based on Reversible Decomposition and Regeneration of Charge-Transfer Complexes. *Cryst. Growth Des* **2022**, *22* (1), 693–702.
- (13) Tian, S.; Huang, Z.; Tan, J.; Cui, X.; Xiao, Y.; Wan, Y.; Li, X.; Zhao, Q.; Li, S.; Lee, C.-S. Manipulating Interfacial Charge-Transfer Absorption of Cocrystal Absorber for Efficient Solar Seawater Desalination and Water Purification. *ACS Energy Lett.* **2020**, *5* (8), 2698–2705.
- (14) Chen, W.; Sun, S.; Huang, G.; Ni, S.; Xu, L.; Dang, L.; Phillips, D. L.; Li, M.-D. Unprecedented Improvement of Near-Infrared Photothermal Conversion Efficiency to 87.2% by Ultrafast Non-Radiative Decay of Excited States of Self-Assembly Cocrystal. *J. Phys. Chem. Lett.* **2021**, *12* (24), 5796–5801.
- (15) Wu, S.; Zhou, B.; Yan, D. Recent Advances on Molecular Crystalline Luminescent Materials for Optical Waveguides. *Adv. Opt. Mater.* **2021**, *9* (23), No. 2001768.
- (16) Xia, X.; Lv, Q.; Xu, C.; Yu, Y.; Wang, L.; Wang, X.; Liao, L. Crafting Near-Infrared Photonics via the Programmable Assembly of Organic Heterostructures at Multiscale Level. *Adv. Funct. Mater.* **2024**, *34* (24), No. 2312478.
- (17) Yu, P.; Li, Y.; Zhao, H.; Zhu, L.; Wang, Y.; Xu, W.; Zhen, Y.; Wang, X.; Dong, H.; Zhu, D.; Hu, W. 1D Mixed-Stack Cocrystals Based on Perylene Diimide toward Ambipolar Charge Transport. *Small* **2021**, *17* (20), No. 2006574.
- (18) Nakabayashi, M.; Matsuo, T.; Hayashi, S. Non-Covalent Supramolecular 1D Alternating Copolymer in Crystal toward 2D Anisotropic Photon Transport. *Chem.—Eur. J.* **2023**, *29* (61), No. e202302351.
- (19) Du, S.; Ma, S.; Xu, B.; Tian, W. Optical Waveguide and Photoluminescent Polarization in Organic Cocrystal Polymorphs. *J. Phys. Chem. Lett.* **2021**, *12* (38), 9233–9238.
- (20) Zhu, W.; Zheng, R.; Zhen, Y.; Yu, Z.; Dong, H.; Fu, H.; Shi, Q.; Hu, W. Rational Design of Charge-Transfer Interactions in Halogen-Bonded Co-Crystals toward Versatile Solid-State Optoelectronics. *J. Am. Chem. Soc.* **2015**, *137* (34), 11038–11046.
- (21) Seki, T.; Kobayashi, S.; Ishikawa, R.; Yano, K.; Matsuo, T.; Hayashi, S. Preparation of Intrinsically Fragile Bent Crystals. *Chem. Sci.* **2024**, *15* (31), 12258–12263.
- (22) Wang, J.; Zhang, S.; Xu, S.; Li, A.; Li, B.; Ye, L.; Geng, Y.; Tian, Y.; Xu, W. Morphology-Dependent Luminescence and Optical Waveguide Property in Large-Size Organic Charge Transfer Cocrystals with Anisotropic Spatial Distribution of Transition Dipole Moment. *Adv. Opt. Mater.* **2020**, *8* (2), No. 1901280.
- (23) Li, S.; Lu, B.; Fang, X.; Yan, D. Manipulating Light-Induced Dynamic Macro-Movement and Static Photonic Properties within 1D Isostructural Hydrogen-Bonded Molecular Cocrystals. *Angew. Chem., Int. Ed.* **2020**, *59* (50), 22623–22630.
- (24) Ma, Y.; Xu, C. F.; Mao, X. R.; Wu, Y.; Yang, J.; Xu, L. P.; Zhuo, M. P.; Lin, H.; Zhuo, S.; Wang, X. D. Oriented Self-Assembly of Hierarchical Branch Organic Crystals for Asymmetric Photonics. *J. Am. Chem. Soc.* **2023**, *145* (16), 9285–9291.
- (25) Lv, Q.; Wang, X. D.; Yu, Y.; Xu, C. F.; Yu, Y. J.; Xia, X. Y.; Zheng, M.; Liao, L. S. Lateral Epitaxial Growth of Two-Dimensional Organic Heterostructures. *Nat. Chem.* **2024**, *16* (2), 201–209.
- (26) Zhang, H.; Lin, D.-Q.; Wu, M.-Z.; Jin, D.; Huang, L.; Xie, L.-H. Multicolor Emission of Organic Microcrystals with Charge Transfer Interactions through Cocrystal Engineering. *Cryst. Growth Des* **2023**, *23* (9), 6548–6556.
- (27) Navarro-Huerta, A.; Hall, D. A.; Blahut, J.; Gómez-Vidales, V.; Teat, S. J.; Marmolejo-Tejada, J. M.; Dračinský, M.; Mosquera, M. A.; Rodríguez-Molina, B. Influence of Internal Molecular Motions in the

- Photothermal Conversion Effect of Charge-Transfer Cocrystals. *Chem. Mater.* **2023**, *35* (23), 10009–10017.
- (28) Harada, J.; Yoneyama, N.; Sato, S.; Takahashi, Y.; Inabe, T. Crystals of Charge-Transfer Complexes with Reorienting Polar Molecules: Dielectric Properties and Order-Disorder Phase Transitions. *Cryst. Growth Des.* **2019**, *19* (1), 291–299.
- (29) Spackman, M. A.; Jayatilaka, D. Hirshfeld Surface Analysis. *CrystEngComm* **2009**, *11* (1), 19–32.
- (30) Liu, Y.; Hu, H.; Xu, L.; Qiu, B.; Liang, J.; Ding, F.; Wang, K.; Chu, M.; Zhang, W.; Ma, M.; Chen, B.; Yang, X.; Zhao, Y. S. Orientation-Controlled 2D Anisotropic and Isotropic Photon Transport in Co-crystal Polymorph Microplates. *Angew. Chem., Int. Ed.* **2020**, *59* (11), 4456–4463.
- (31) Yao, W.; Yan, Y.; Xue, L.; Zhang, C.; Li, G.; Zheng, Q.; Zhao, Y. S.; Jiang, H.; Yao, J. Controlling the Structures and Photonic Properties of Organic Nanomaterials by Molecular Design. *Angew. Chem., Int. Ed.* **2013**, *52* (33), 8713–8717.
- (32) Li, Q.; Jin, W.; Chu, M.; Zhang, W.; Gu, J.; Shahid, B.; Chen, A.; Yu, Y.; Qiao, S.; Zhao, Y. S. Tailoring the Structures and Photonic Properties of Low-Dimensional Organic Materials by Crystal Engineering. *Nanoscale* **2018**, *10* (10), 4680–4685.
- (33) Zhuo, M.; Tao, Y.; Wang, X.; Wu, Y.; Chen, S.; Liao, L.; Jiang, L. 2D Organic Photonics: An Asymmetric Optical Waveguide in Self-Assembled Halogen-Bonded Cocrystals. *Angew. Chem., Int. Ed.* **2018**, *57* (35), 11300–11304.
- (34) Hino, Y.; Matsuo, T.; Hayashi, S. Unique 2D Face Topologies in Naphthyl-Appended Naphtho[k]Fluoranthene-Based 3D Crystals for Optical Waveguide. *Adv. Opt. Mater.* **2023**, *11* (13), No. 2201810.
- (35) Hernández, F. J.; Crespo-Otero, R. Excited State Mechanisms in Crystalline Carbazole: The Role of Aggregation and Isomeric Defects. *J. Mater. Chem. C* **2021**, *9* (35), 11882–11892.
- (36) Dommett, M.; Rivera, M.; Crespo-Otero, R. How Inter- and Intramolecular Processes Dictate Aggregation-Induced Emission in Crystals Undergoing Excited-State Proton Transfer. *J. Phys. Chem. Lett.* **2017**, *8* (24), 6148–6153.
- (37) Rivera, M.; Stojanović, L.; Crespo-Otero, R. Role of Conical Intersections on the Efficiency of Fluorescent Organic Molecular Crystals. *J. Phys. Chem. A* **2021**, *125* (4), 1012–1024.
- (38) Perdew, J. P.; Burke, K.; Ernzerhof, M. Generalized Gradient Approximation Made Simple. *Phys. Rev. Lett.* **1996**, *77* (18), 3865–3868.
- (39) Zhao, Y.; Truhlar, D. G. The M06 Suite of Density Functionals for Main Group Thermochemistry, Thermochemical Kinetics, Noncovalent Interactions, Excited States, and Transition Elements: Two New Functionals and Systematic Testing of Four M06-Class Functionals and 12 Other Functionals. *Theor. Chem. Acc.* **2008**, *120* (1–3), 215–241.
- (40) Frisch, M. J.; Trucks, G. W.; Schlegel, H. B.; Scuseria, G. E.; Robb, M. A.; Cheeseman, J. R.; Scalmani, G.; Barone, V.; Mennucci, B.; Petersson, G. A.; Nakatsuji, H.; Caricato, M.; Li, X.; Hratchian, H. P.; Izmaylov, A. F.; Bloino, J.; Zheng, G.; Sonnenberg, J. L.; Hada, M.; Ehara, M.; Toyota, K.; Fukuda, R.; Hasegawa, J.; Ishida, M.; Nakajima, T.; Honda, Y.; Kitao, O.; Nakai, H.; Vreven, T.; Montgomery, J. A., Jr.; Peralta, J. E.; Ogliaro, F.; Bearpark, M.; Heyd, J. J.; Brothers, E.; Kudin, K. N.; Staroverov, V. N.; Kobayashi, R.; Normand, J.; Raghavachari, K.; Rendell, A.; Burant, J. C.; Iyengar, S. S.; Tomasi, J.; Cossi, M.; Rega, N.; Millam, J. M.; Klene, M.; Knox, J. E.; Cross, J. B.; Bakken, V.; Adamo, C.; Jaramillo, J.; Gomperts, R.; Stratmann, R. E.; Yazyev, O.; Austin, A. J.; Cammi, R.; Pomelli, C.; Ochterski, J. W.; Martin, R. L.; Morokuma, K.; Zakrzewski, V. G.; Voth, G. A.; Salvador, P.; Dannenberg, J. J.; Dapprich, S.; Daniels, A. D.; Farkas, Ö.; Foresman, J. B.; Ortiz, J. V.; Cioslowski, J.; Fox, D. J. *Gaussian 09* Revision E.01, Gaussian, Inc.: Wallingford.
- (41) Eaton, S. S.; Eaton, G. R. Relaxation Times of Organic Radicals and Transition Metal Ions. In *Distance Measurements in Biological Systems by EPR*; Berliner, L. J.; Eaton, G. R.; Eaton, S. S., Ed.; Springer US: Boston, MA, 2000; pp 29–154.
- (42) Jiang, M.; Li, S.; Zhen, C.; Wang, L.; Li, F.; Zhang, Y.; Dong, W.; Zhang, X.; Hu, W. TCNQ-Based Organic Cocrystal Integrated Red Emission and n-Type Charge Transport. *Front. Optoelectron.* **2022**, *15* (1), 1–10.
- (43) Goud, N. R.; Matzger, A. J. Impact of Hydrogen and Halogen Bonding Interactions on the Packing and Ionicity of Charge-Transfer Cocrystals. *Cryst. Growth Des.* **2017**, *17* (1), 328–336.
- (44) Jin, M.; Chung, T. S.; Seki, T.; Ito, H.; Garcia-Garibay, M. A. Phosphorescence Control Mediated by Molecular Rotation and Auophilic Interactions in Amphidynamic Crystals of 1,4-Bis[Tri-(p-Fluorophenyl)Phosphane-Gold(I)-Ethyne]Benzene. *J. Am. Chem. Soc.* **2017**, *139* (49), 18115–18121.
- (45) Fahey, D. P.; Dougherty, W. G.; Kassel, W. S.; Wang, X.; Beckmann, P. A. Nonexponential Solid State ^1H and ^{19}F Spin-Lattice Relaxation, Single-Crystal X-Ray Diffraction, and Isolated-Molecule and Cluster Electronic Structure Calculations in an Organic Solid: Coupled Methyl Group Rotation and Methoxy Group Libration in 4,4'-Dimethoxyoctafluorobiphenyl. *J. Phys. Chem. A* **2012**, *116* (48), 11946–11956.
- (46) Beckmann, P. A.; Rosenberg, J.; Nordstrom, K.; Mallory, C. W.; Mallory, F. B. CF_3 Rotation in 3-(Trifluoromethyl)Phenanthrene: Solid State ^{19}F and ^1H NMR Relaxation and Bloch–Wangsness–Redfield Theory. *J. Phys. Chem. A* **2006**, *110* (11), 3947–3953.
- (47) Aguilar-Granda, A.; Pérez-Estrada, S.; Roa, A. E.; Rodríguez-Hernández, J.; Hernández-Ortega, S.; Rodríguez, M.; Rodríguez-Molina, B. Synthesis of a Carbazole-[π]-Carbazole Molecular Rotor with Fast Solid State Intramolecular Dynamics and Crystallization-Induced Emission. *Cryst. Growth Des.* **2016**, *16* (6), 3435–3442.